Elsevier Editorial System(tm) for Journal of Alloys and Compounds

Manuscript Draft

Manuscript Number:

Title: Synthesis, Structure and Complex Study of Properties of EuErCuS3

Article Type: Full Length Article

Keywords: inorganic materials; thermochemistry; spectroscopy; magnetic measurements; optical spectroscopy; X-ray diffraction.

Corresponding Author: Professor Anna Ruseykina, Ph.D

Corresponding Author's Institution:

First Author: Anna Ruseykina, Ph.D

Order of Authors: Anna Ruseykina, Ph.D; Leonid Solovyov; Vladimir Chernyshev; Aleksandr Aleksandrovsky; Oleg Andreev; Svetlana Krylova; Alexander Krylov; Dmitriy Velikanov; Maxim Molokeev; Nikolai Maximov; Maxim Grigoriev; Alexander Garmonov; Aleksei Matigorov

Abstract: The crystal structure of the first-synthesized compound EuErCuS3 was determined from X-ray powder diffraction data: orthorhombic crystal system, space group Pnma, structural type Eu2CuS3: a = 10.1005(2) Å, b = 3.91255(4) Å, c = 12.8480(2) Å; V = 507.737(14) Å3, Z = 4, and ρx = 6.266g/cm3. The temperatures and enthalpies of reversible polymorphic transitions and of incongruent melting of the compound were determined by DSC: Tα↔β= 1524 K, ΔHα↔β = 2.3±0.2 kJ·mol-1;Tβ↔γ = 1575 K, ΔHβ↔γ = 0.7±0.1 kJ·mol-1;Tγ↔δ=1602 K; ΔHγ↔δ= 1.3±0.1 kJ·mol-1; and Tm =1740±6 K, ΔHcr=-3.5±0.3 kJ·mol-1.IR spectra were recorded in the range from 50 to 400 cm-1. The compound was found to be IR-transparent in the range 4000-400 cm-1. The compound was characterized by Raman spectroscopy. The observed spectra featured both Raman lines and luminescence. Ab initio calculations of the EuErCuS3 crystal structure and phonon spectrum were performed, the frequencies and types of fundamental modes were determined, and the involvement of constituent ions in the IR and Raman modes was assessed from an analysis of the ab initio displacement vectors. The vibrational spectra were interpreted. EuErCuS3 experiences a ferromagnetic transition at 4.8K. Its microhardness is 2850MPa. The data obtained can serve as the basis for predicting the properties of EuLnCuS3 compounds. Valence states for Eu (2+) and Er (3+) are proved both by XRD and optical methods.

Prime Novelty Statement

The prime novelty of this research is the complex study of the crystal structure and multifunctional properties of $EuErCuS_3$ multication sulfide. The crystals compound are orthorhombic symmetry which melts incongruently. This compound has a 3 high-temperature polymorphic transitions and is a wide-gap semiconductor which contains the magnetic ion Er^{3+} experiencing a low-temperature ferromagnetic transition. Valence state of Eu^{2+} ion is determined via XRD and optical techniques. Ab initio calculations of the $EuErCuS_3$ crystal structure and phonon spectrum were performed, the frequencies and types of fundamental modes were determined, and the involvement of constituent ions in the IR and Raman modes was assessed from an analysis of the ab initio displacement vectors.

Synthesis, Structure and Complex Study of Properties of $EuErCuS_3$

Anna V. Ruseikina[a], Leonid A. Solovyov[b], Vladimir A. Chernyshev[c],AleksandrS. Aleksandrovsky[d,e], Oleg V. Andreev[a], Svetlana N. Krylova[d], Alexander S. Krylov[d], DmitriyA. Velikanov[d], Maxim S. Molokeev[f,g], Nikolai G. Maximov[h], Maxim V. Grigoriev[a], Alexander A. Garmonov[i], Alexey V. Matigorov[a]

[a]Institute of Chemistry, University of Tyumen, Tyumen 625003, Russia

[b]Institute of Chemistry and Chemical Technology, Federal Research Center KSC SB RAS, Krasnoyarsk660049, Russia

[c]Institute of Natural Sciences and Mathematics, Ural Federal University, Ekaterinburg 620002, Russia

[d]Laboratory of Coherent Optics, Kirensky Institute of Physics, Federal Research Center KSC SB RAS, Krasnoyarsk 660036, Russia

[e]Department of Photonics and Laser Technologies, Siberian Federal University, Krasnoyarsk 660079, Russia

[f]Laboratory of Crystal Physics, Kirensky Institute of Physics, Federal Research Center KSC SB RAS, Krasnoyarsk 660036, Russia

[g]Siberian Federal University, Krasnoyarsk 660079, Russia

[h]Institute of Chemistry and Chemical Technology SB RAS, Federal Research Center "Krasnoyarsk Science Center SB RAS"

[i]Institute of Physics and Technology, University of Tyumen, Tyumen 625003, Russia

Corresponding author:
Institute of Chemistry, University of Tyumen, Perekopskaya 15a, Tyumen 625003, Russia
Phone: 89129905701
E-mail: adeschina@mail.ru

Abstract

The crystal structure of the first-synthesized compound $EuErCuS_3$ was determined from X-ray powder diffraction data: orthorhombic crystal system, space group Pnma, structural type Eu_2CuS_3: a = 10.1005(2)Å, b = 3.91255(4)Å, c = 12.8480(2) Å; V = 507.737(14) $Å^3$, Z = 4, and ρ_x = 6.266 g/cm^3. The temperatures and enthalpies of reversible polymorphic transitions and of incongruent melting of the compound were determined by DSC: $T_{\alpha\leftrightarrow\beta}$= 1524 K, $\Delta H_{\alpha\leftrightarrow\beta}$ = 2.3±0.2 $kJ\cdot mol^{-1}$; $T_{\beta\leftrightarrow\gamma}$ = 1575 K, $\Delta H_{\beta\leftrightarrow\gamma}$ = 0.7±0.1 $kJ\cdot mol^{-1}$; $T_{\gamma\leftrightarrow\delta}$=1602 K; $\Delta H_{\gamma\leftrightarrow\delta}$ = 1.3±0.1 $kJ\cdot mol^{-1}$ and T_m =1740±6 K, ΔH_{cr} = -3.5±0.3 $kJ\cdot mol^{-1}$. IR spectra were recorded in the range from 50 to 400 cm^{-1}. The compound was found to be IR-transparent in the range 4000–400 cm^{-1}. The compound was characterized by Raman spectroscopy. The observed spectra featured both Raman lines and luminescence. Ab initio calculations of the $EuErCuS_3$ crystal structure and phonon spectrum were performed, the frequencies and types of fundamental modes were determined, and the involvement of constituent ions in the IR and Raman modes was assessed from an analysis of the ab initio displacement vectors. The vibrational spectra were interpreted. $EuErCuS_3$ experiences a ferrimagnetic transition at 4.8K. Its microhardness is 2850 MPa. The data obtained can serve as the basis for predicting the properties of $EuLnCuS_3$ compounds. Valence states for Eu (2+) and Er (3+) are proved both by XRD and optical methods.

Keywords: inorganic materials; thermochemistry; spectroscopy; magnetic measurements; optical spectroscopy; X-ray diffraction.

1. Introduction

Complex rare-earth chalcogenides $ALnCuS_3$ (A^{2+} = Pb, Eu, Sr, or Ba) have specific electric [1–6], thermal [7–11], magnetic [1,12–14], and optical[1,8,11,14] properties. X-ray powder diffraction experiments on samples annealed at 1170 K showed three types of orthorhombic crystal

structures to exist in the $EuLnCuS_3$ (Ln = La-Ho, Tm-Lu) series[12,15,16] (Table 1).

Table 1

Structural types (STs) of $EuLnCuS_3$ (Ln = La-Lu) compounds determined in samples annealed at 1170 K.

$EuLnCuS_3$ structural type												
La	Ce	Pr	Nd	Sm	Gd	Tb	Dy	Ho	Er	Tm	Yb	Lu
									-			

The background cell coloring denotes the structural type (ST) in which the $EuLnCuS_3$ compound crystallizes: crosshatched cells – Eu_2CuS_3ST, dark gray cells – Ba_2MnS_3ST, horizontal-striped cells – $KZrCuS_3$ST, and hyphenated white cells – an undetermined ST.

The $EuLnCuS_3$ (Ln = Tb, Dy, and Tm) compounds that contain magnetic Ln^{3+} ions experience a ferrimagnetic transition at 5.4, 5.3, and 5.4K, respectively; in the compounds containing nonmagnetic Ln^{3+}ions (Ln = Y, Eu, and Lu), ferromagnetic ordering of Eu^{2+}moments occurs at 3.4–4.4 K [12,13].

The $ALnCuS_3$ (A = Sr, Eu; Ln = Gd, Dy, and Ho) compounds experience three polymorphic transitions at temperatures above 1400 K upon heating and cooling as shown by differential scanning calorimetry (DSC) [7,17,18]. For $EuHoCuS_3$, the polymorphic transition temperatures and enthalpies are $T_{\alpha\leftrightarrow\beta}$= 1516 K, $\Delta H_{\alpha\leftrightarrow\beta}$=3.7 kJ/mol; $T_{\beta\leftrightarrow\gamma}$=1562 K, $\Delta H_{\beta\leftrightarrow\gamma}$=1.2 kJ/mol; and $T_{\gamma\leftrightarrow\delta}$ = 1591 K, $\Delta H_{\gamma\leftrightarrow\delta}$= 2.2 kJ/mol [17]. High-temperature polymorphs have not been obtained by cooling or quenching. The $EuLnCuS_3$ compounds melt incongruently: $EuLaCuS_3$ (1539±4 K), $EuCeCuS_3$ (1524±3 K), $EuPrCuS_3$ (1497±3 K), $EuNdCuS_3$ (1470±4K) [8, 16]), $EuGdCuS_3$ (1720±5 K) [7], $EuHoCuS_3$ (1721±5 K) [17] and $EuDyCuS_3$ (1721±4K) [18].

We failed to find any piece of data on the crystal structure, thermal, optical, or magneticproperties of $EuErCuS_3$ in the literature.

The goals of this study were to prepare the compound $EuErCuS_3$ and to determine its structure, to characterize it by physicochemical methods, and to determine its optical and magnetic properties. Special goal is connected with the check of valence states of two rare earth ions, Eu and Er, in the crystal structure under investigation. It is known that most stable valence of RE ions is 3+, and if no precautions are taken, they tend to attain this valence state even while occupying sites with nominal valence 2+, due to inclusion of, e.g, oxygen-containing defects, like in case of doping of fluorite crystals with RE. Some hosts are especially favorable for stabilizing divalent RE ions like single crystalline alpha-SBO doped with europium, In the case of the crystal structure under consideration, i.e., $EuErCuS_3$, the competition between Eu and Er for occupying either divalent or trivalent positions maybe of interest. It must be noted that in earlier studied compounds (see references above) Eu is found to be in divalent state, in accordance with the additional stability of f^7 shell of Eu^{2+} ion. In the compound under study the investigation of valence states of RE ions can be done with the help of XRD or optical spectroscopy.

2. Experimental

The compound $EuErCuS_3$ was prepared by alloying a batch of composition $2EuS : 1Er_2S_3 : 1Cu_2S$ [16–18]. Cu_2S was prepared by heating the constituent elements (Cu (99.99 wt.%,Russia) and S (99.99 wt.%, Russia)) to 1420 K for 24 hin an evacuated and sealed-off double-walled silica glass ampoule, followed by 30-min isothermal exposure at this temperature. The thus-prepared Cu_2S sample was orthorhombic, space group Ab2m[19], with the unit cell parameters a = 13.53(3)Å, b = 27.47(3)Å, c = 11.88(1)Å. The DSC curves for this sample featured peaks that corresponded to the polymorphic transitions $\alpha\text{-}Cu_2S \rightarrow \beta\text{-}Cu_2S$ at 376 K and $\beta\text{-}Cu_2S \rightarrow \gamma\text{-}Cu_2S$ at 708 K and the melting peak of the compound at 1402 K,

in agreement with [20].Single-phase EuS and Er_2S_3 samples were prepared from Ln_2O_3 (99.99 wt.%, China) in an H_2S and CS_2 flow at 1300 K [15,21,22]. δ-$Er_2S_3$is a monoclinic compound, space group $P2_1/m$ [23,24], with a = 17.42(2) Å, b = 3.976(4) Å, c = 10.04(1) Å, β = 98.5(5)°. EuS is cubic, space group Fm3m [25,26], with a = 5.968(1) Å. The lanthanide-to-sulfur ratio in the compounds as probed by SEM corresponded to the EuS and Er_2S_3 stoichiometries within the SEM error bar. A2EuS: $1Er_2S_3$:$1Cu_2S$ batch was pounded in an agate mortar and then alloyed in a graphite crucible placed inside an argon (99.998 wt.%, Russia)-filled silica glass reactor, or in an evacuate and sealed-off silica glass ampoule. As-synthesized samples were annealed in evacuatedand sealed-off silica glass ampoules at 1170 K for 1500 hours [15,27].

X-ray diffraction experiments were carried out on a DRON-7 diffractometer and a PANalytical X'Pert PRO diffractometer both equipped with a PIXceldetector (Fe-filtered CoK_α radiation). The X-ray diffraction patterns were scanned at 298 K over the angle range $10^o \leqslant 2\theta \leqslant 125(145)$ with 0.013^osteps; the total accumulation time was 13 h. Unit cell parameters were determined in the ITO program[28]. The observed systematic absences showed that the $EuErCuS_3$ structure (after annealing at 1170 K) belongs to space group Pnma (for general reflections hkl, no systematic absences were observed, so the unit cell isprimitive; for reflections 0kl: k + l= 2n; for hk0: h= 2n; for h00: h = 2n; for 0k0: k= 2n; and for 00l: l = 2n). The initial model used was the dataset for the isostructural compound Eu_2CuS_3 [29]. The crystal structure was refined by the difference derivative minimization (DDM) method [30] in the anisotropic approximation for all atoms with account for preferred orientation, anisotropic peak broadening, surface roughness and displacement (R_{DDM}= 5.3%; R_{Bragg} = 2.9 %). Apart from the major phase, the refined model included identified microimpurities: 1 wt.% Er_2O_2S. Phase identification was with reference to the ICDDPDF4+2012

file. Crystal structures were visualized in the program package Diamond 3 [31].

Microstructures were observedon polished samples using an AxioVert.A1 metallurgical microscope. Scanning electron microscopy (SEM) experiments were carried out on a JEOLJSM-6510 LV equipped with an energy-dispersive X-ray spectral analyzer. The element determination precision was 0.5 wt%.

Differential scanning calorimetry experiments were carried out on a Setsys Evolution 1750 (TG–DSC 1600) complex using a PtRh 6%-PtRh 30%thermocouple. The complex was calibrated against the melting temperatures and melting enthalpies of references (Sn, Pb, Zn, Al, Ag, Au, Cu, and Pd). Prior to an experiment, the working chamber of the complex was evacuated and then filled with argon. The recording parameters were the following: the sample size: 100-110 mg, heating rate: 5 K/min, argon flow rate: 25 mL/min, and alundum crucible capacity: 100 μL. The heat absorption onset temperature was determined as the intersection point of a tangent with the baseline in the program package Setsoft Software 2000 with a linear baseline from first to last point. The temperatures and enthalpies of the thermal events appearing in replica measurements fell within the thermoanalytical error bar. TG curves showed a 0.025 wt. % weight loss in a $EuErCuS_3$ sample in the range 1678–1745 K.

A durometric analysis of a polished sample was performed by the Vickers method on an HMV-G21 [32]. The exposure time was 15 s; the load was 10 kg-force(98.07 N).

The room-temperature magnetic properties of $EuErCuS_3$ were studied on a vibrating sample magnetometer with a Puzey electromagnet [33]. The sample weight was 0.0543 g. Low-temperature magnetic susceptibility was studied on a SQUID magnetometer [34] in a 10-Oe magnetic field. Temperature-dependent magnetic susceptibility was

measured inthe ZFC(zero-field cooling) and FC (nonzero-field cooling) modes.

IR spectra in the range 600–50 cm^{-1} were recorded with 2-cm^{-1} resolution on a VERTEX 70V (BRUKER) FT-IR vacuum spectrometer equipped with a SiC IR source and an RT-DTGS detector with a polyethylene window and a T240/3wide-band amplifier. Prior to measurements the spectrometer was evacuated to a residual pressure of less than 0.2 gPa. A cast complex sulfide sample was pounded in an agate mortar; the thus-prepared powder was placed on a diamond crystal of a Platinum ATR single-reflection ATR accessory for measurements.

IR absorption spectra in the range 4000–400 cm^{-1}were measured on a FTIR spectral Varian Excalibur HE 3600.

Raman spectra were excited by polarized 514.5-nm and 457.9-nm beams of a Spectra-Physics Stabilite 2017 200-mW argon laser(250 μW on the test sample). The laser beam was focused on the test sample by an Olympus BX41 updated microscope through an OlympusMPlan100xobject lens with the digital aperture 0.9. The scattered beam was collected through the same object lens and targeted to the spectrometer. Spectra in the 180° (back-scattered) geometry were obtained on a HoribaJobinYvon T64000 spectrometer with a triple monochromator in the dispersion subtraction mode in the frequency range 15–3600 cm^{-1}. The detector used was a liquid nitrogen-cooled CCD matrix. The focused laser beam diameter was ~2 μm.

The ab initio calculations of the $EuErCuS_3$ crystal structure and phonon spectrum werecarried out in the frame of density functional theory (DFT) [35] using the B3LYP exchange-correlation functional [36,37] to take into account both local and nonlocal Hartree−Fock exchanges. The calculations were carried out in the program CRYSTAL14 [38,39]. For europium and erbium, the ECP53MWB and ECP57MWB quasi-relativistic pseudo-potentials [40,41] were used with the attached valence basis set ECP53MWB and ECP57MWB-I, respectively [42]. The Gaussian primitives

with exponents less than 0.1 were removed from the basis sets. For copper, the full-electron basis set [43] was used, available on the CRYSTAL program site as «Cu_86-4111(41D)G_doll_2000» [39]. For sulfur, the DURAND pseudo-potential with the attached valence basis set was used [39,44]. The exponents in the two outer orbitals of the valence basis set were changed to 0.24 and 0.27. The use of pseudo-potentials for the description of coreelectronic shells of rare-earth ions, the 4f shell inclusive, with the valence orbitals involved in chemical bonding described by valence basis sets, makes it possible to successfully reconstitute the lattice structure and lattice dynamics in the compounds that have a lanthanide ion sublattice [45,46]. The crystal structure was first calculated, followed by phonon spectrum calculations for crystal structure optimization. Calculation details are found elsewhere [45].

Diffuse reflection spectrum of $EuErCuS_3$ was measured using Shimadzu UV-3600 spectrometer.

3. **Results and discussion**

3.1. Crystal Structure

The $EuErCuS_3$ diffraction pattern (Fig. 1) was indexed in terms of orthorhombic space group Pnma, Eu_2CuS_3 structural type, with the unit cell parameters a = 10.1005(2) Å, b = 3.91255(4) Å, c = 12.8480(2) Å; V = 507.737(14) $Å^3$, Z = 4, ρ_x = 6.266 g/cm^3. The unit cell parameters calculated in the DFT frame with the B3LYP functional (a = 10.126 Å, b= 3.896 Å, c =12.600 Å) correlated with the experimental values.

The $EuErCuS_3$ structure is described by two-dimensional layers ($CuErS_3$) in plane b–a built of distorted tetrahedra CuS_4 and octahedral ErS_6, with Eu^{2+} ions in between. The crystal data and selected interatomic distances for $EuErCuS_3$ are listed in Table 1 and Table 2, respectively. The structural parameters are in Table 3.

Table 1.

Atomic coordinates in the $EuErCuS_3$ structure.

Atom	x	y	z
Eu	0.76479(16)	0.25	0.00169(9)
Er	0.01020(11)	0.25	0.74489(9)
Cu	0.24037(24)	0.25	0.22147(14)
S1	0.05556(47)	0.25	0.11536(34)
S2	0.42054(49)	0.25	0.10848(35)
S3	0.25808(44)	0.25	0.82710(28)

Table 2.

Anisotropic thermal parameters ($Å^2$) in the $EuErCuS_3$ structure

Atom	U^{11}	U^{22}	U^{33}	U^{12}	U^{13}	U^{23}
Eu	0.0249(16)	0.0109(14)	0.0105(14)	0.0000	0.0002(9)	0.0000
Er	0.0106(13)	0.0065(13)	0.0083(12)	0.0000	-0.0015(6)	0.0000
Cu	0.0100(18)	0.0116(19)	0.0138(18)	0.0000	0.0026(16)	0.0000
S1	0.0103(29)	0.0128(47)	0.0059(33)	0.0000	-0.0008(23)	0.0000
S2	0.0111(35)	0.0047(49)	0.0092(32)	0.0000	0.0011(23)	0.0000
S3	0.0027(25)	0.0066(28)	0.0124(21)	0.0000	-0.0022(29)	0.0000

Table 3.

Interatomic distances (d) in the $EuErCuS_3$ structure.

Bond	d, Å	Bond	d, Å	Bond	d, Å
Eu—$S1^{i}$	3.2800(49)	Er—$S1^{iv}$	2×2.7372(32)	Cu—S1	2.312(5)
Eu—$S1^{ii}$	2×3.0629(37)	Er—$S2^{v}$	2×2.7181(33)	Cu—S2	2.328(5)
Eu—$S2^{ii}$	2×3.0552(39)	Er—S3	2.7174(45)	Cu—$S3^{vii}$	2×2.3810(23)
Eu—$S3^{iii}$	2×2.9529(29)	Er—$S3^{vi}$	2.7093(45)	<Cu—S>	2.350(2)
<Eu—S>	3.060(2)	<Er—S>	2.723(2)		

The parenthesized values are mean interatomic distances. Symmetric positions: (i) 1+x, y, z; (ii) 1-x, -0.5+y, -z; (iii) 1-x, -0.5+y, 1-z; (iv) -x, -0.5+y, 1-z; (v) 0.5-x, -y, 0.5+z; (vi) -0.5+x, 0.5-y, 1.5-z; (vii) 0.5-x, -y, -0.5+z; (viii) 1-x, 0.5+y, -z; (ix) 1-x, 0.5+y, 1-z; (x) -x, 0.5+y, 1-z; (xi) 0.5-x, 1-y, 0.5+z; and (xii) 0.5-x, 1-y, -0.5+z

Table 4.

Selected bond angles in the $EuErCuS_3$ structure.

Angle	ω, deg	Angle	ω, deg
$S1^{i}$—Eu—$S1^{ii}$	71.83(11)	$S1^{iv}$—Er—$S2^{v}$	88.34(10)
$S1^{i}$—Eu—$S2^{ii}$	139.01(7)	$S1^{iv}$—Er—$S2^{xi}$	178.90(14)
$S1^{i}$—Eu—$S3^{iii}$	74.83(11)	$S1^{iv}$—Er—S3	88.20(12)
$S1^{ii}$—Eu—$S1^{viii}$	79.39(11)	$S1^{iv}$—Er—$S3^{vi}$	89.76(12)
$S1^{ii}$—Eu—$S2^{ii}$	74.13(11)	$S2^{v}$—Er—$S2^{xi}$	92.06(14)
$S1^{ii}$—Eu—$S2^{viii}$	122.99(12)	$S2^{v}$—Er—S3	90.77(12)
$S1^{ii}$—Eu—$S3^{iii}$	89.37(9)	$S2^{v}$—Er—$S3^{vi}$	91.25(12)
$S1^{ii}$—Eu—$S3^{ix}$	146.64(13)	S3—Er—$S3^{vi}$	177.09(9)
$S2^{ii}$—Eu—$S2^{viii}$	79.63(12)	S1—Cu—S2	105.28(18)
$S2^{ii}$—Eu—$S3^{iii}$	82.7(1)	S1—Cu—$S3^{vii}$	109.97(13)
$S2^{ii}$—Eu—$S3^{ix}$	136.17(13)	S2—Cu—$S3^{vii}$	110.51(13)
$S3^{iii}$—Eu—$S3^{ix}$	82.98(10)	$S3^{vii}$—Cu—$S3^{xii}$	110.50(16)
$S1^{iv}$—Er—$S1^{x}$	91.24(14)		

According to the bond valence sum calculations [47] given in Table 5, the valence states of Eu, Er and Cu ions in $EuErCuS_3$ are close to 2, 3 and 1, respectively.

Table 5. Bond valence calculations for Eu, Er and Cu in $EuErCuS_3$.

Bond	Dist., Å	R, Å	B	BVal
Eu—S3	2.953	2.584	0.37	0.369
Eu—S3	2.953	2.584	0.37	0.369
Eu—S2	3.055	2.584	0.37	0.280
Eu—S2	3.055	2.584	0.37	0.280
Eu—S1	3.063	2.584	0.37	0.274
Eu—S1	3.063	2.584	0.37	0.274
Eu—S1	3.281	2.584	0.37	0.152
			Sum	1.998
Er—S3	2.709	2.460	0.37	0.510
Er—S3	2.718	2.460	0.37	0.498
Er—S2	2.718	2.460	0.37	0.498
Er—S2	2.718	2.460	0.37	0.498
Er—S1	2.737	2.460	0.37	0.473
Er—S1	2.737	2.460	0.37	0.473
			Sum	2.950
Cu—S1	2.311	1.898	0.37	0.328
Cu—S2	2.327	1.898	0.37	0.314
Cu—S3	2.381	1.898	0.37	0.271
Cu—S3	2.381	1.898	0.37	0.271
			Sum	1.183

A $EuErCuS_3$ powder consists of planar particles with linear sizes of 1 to 10 μm (Fig. 3). Elemental distribution spectra were recorded at five surface spots of the sample. The chemical composition of the sample agrees with the theoretical contents of the elements.

3.2.Thermal Properties and Microhardness

The DSC heating curves for a polycrystalline $EuErCuS_3$ sample feature three endotherms in the range 1524-1610 K induced by first-order phase transformations, namely, polymorphic transitions (Fig. 3). Similar transitions were detected in $ALnCuS_3$ (A = Sr or Eu) isostructural compounds [7,17]. The polymorphs of the compound are denoted in the increasing order of temperatures as and $EuErCuS_3$. The temperatures and enthalpies of phase transitions are listed in Table 6.

Table 6.

Physicochemical characteristics of $EuErCuS_3$

Temperatures (K) and enthalpies ($kJ \cdot mol^{-1}$) of phase transitions								
$T_{\alpha\leftrightarrow\beta}$	$\Delta H_{\alpha\leftrightarrow\beta}$	$T_{\beta\leftrightarrow\gamma}$	$\Delta H_{\beta\leftrightarrow\gamma}$	$T_{\gamma\leftrightarrow\delta}$	$\Delta H_{\gamma\leftrightarrow\delta}$	T_m	ΔH_{cr}
1524±2	2.3±0.2	1575±3	0.7±0.1	1602±3	1.3±0.1	1740±6*	-3.5±0.3

X_{obs}, $emu \cdot mol^{-1}$	C, $emu \cdot K \cdot mol^{-1}$		Band gap, eV		Sample color	H, MPa	T_c,K	
	obs	calc	obs	calc			obs	calc
0.0636	19.46	19.36	1.93	2.56	Red-brown	2850±150	4.8±0.2	5.0

*As shown by DSC cooling curves.

The phase transitions occur within a narrow temperature range less than 10 K. The thermal features are completely reproduced upon cooling, so the transitions may be regarded to be rapid. Quenching of samples to aqueous NaCl solutions failed to yield high-temperature phases of the compound.

$EuErCuS_3$ melts incongruently to yield polycrystalline EuS and a melt. A melt-crystallized sample had a microstructure represented by EuS

primary grains, light brown $EuErCuS_3$ crystals, and a eutectic between tie-lined $ErCuS_2$ and $EuErCuS_3$ phases. The crystallization peak was separated into components, namely, the heat of formation of EuS primary crystals and the heat of formation of a $EuErCuS_3$ phase. A tentative value of the $EuErCuS_3$ enthalpy of crystallization was determined taking into account the phase composition of a cooled sample (Table6).

The microhardness value measured for $EuErCuS_3$ (Table6) exceeds the microhardness of isoformula compounds (for $EuLaCuS_3$, H = 2050 MPa [16]), in correlation with the decreasing Ln^{3+} radii.

3.3. Magnetic Properties

A magnetic moment versus magnetic field plot for $EuErCuS_3$ was constructed by 768 datapoints in the range from 0to 9650 Oe (Fig. 4). The magnetic field was varied in 10-20 Oe steps. The 298 K magnetic moment of the test sample rises linearly with field intensity, a trend typical of a paramagnetic state. The molar magnetic susceptibility χ was calculated from the plot (Fig. 4, Table6).

The temperature-dependent magnetic susceptibility below 14 K shows a transition to an ordered anisotropic magnetic structure at 4.8±0.2 K (Fig.5). The reciprocal magnetic susceptibility near the phase transition departs from the linear trend; this departure is typical for ferrimagnets and correlates with a similar behavior observed for $EuGdCuS_3$ (where the transition temperatureis 5.37 K [12]).

In Néel' theory, the temperature-dependent reciprocal magnetic susceptibility fora two-sublattice ferrimagnet is described by the relationship [48]

$$\frac{1}{\chi} = \frac{T}{C} + \frac{1}{\chi_0} - \frac{\sigma}{T-\theta} \quad (1)$$

Where C is Curie's constant; and χ_0, σ, and θ are the fitting parameters (including C).

Processing of the experimental data (Fig.5) gave a value of 19.46 emu·K·mol^{-1} for C (for $EuGdCuS_3$, C = 15.51 emu·K·mol^{-1} [12]). The relationship $C = \frac{N_A}{3k}\left(\mu_{Eu}^2 + \mu_{Er}^2\right)$ (where μ is the magnetic moment equal to 7.94 μ_B and 9.58 μ_B for Eu^{2+} and Er^{3+}, respectively [49,50]) gave C = 19.36 emu·K·mol^{-1} for the paramagnetic state of $EuErCuS_3$. The thus-calculated values of Curie's constant were used to calculate χ for 298 K: 0.0655 and 0.0652 emu·mol^{-1}; these χ values coincide, to within 3%, with the experimentally determined value χ = 0.0636 emu·mol^{-1} (for $EuGdCuS_3$, $\chi \approx 0.05$ emu·mol^{-1} [12]). The calculations of the Curie temperature (at which $\frac{1}{\chi} = 0$) through the parameters (C, χ_0, σ, and θ) of model (1) by the relationship (2) give T_c = 5.0 K.

$$T_c = \theta - \frac{C}{\chi_0} + \frac{1}{2}\sqrt{\left(\theta - \frac{C}{\chi_0}\right)^2 + 4C\left(\frac{\theta}{\chi_0} + \sigma\right)} \quad (2)$$

3.4. Vibrational Spectroscopy

Figure 6 shows Raman spectra recorded at various excitation wavelengths. The noticeable differences between the observed spectra indicate that luminescence spectra were recorded together with the vibrational spectrum. The joint analysis of these spectra makes it possible to exclude the luminescence contribution and recognize the lines that reliably belong to the vibrational frequencies of the crystal unit cell.

Selection rules were calculated for interpreting the observed vibrational spectra. The result is shown in Table 7. The crystal belongs to space group Pnma. According to the calculations, 36 modes were expected to appear in the Raman spectrum and 27 modes in IR absorption spectra.

Table 7.

Wyckoff positions, irreducible representations, classification of modes, and Raman tensors for $EuErCuS_3$ (space group Pnma, No.62)

Atom	Wyckoff position	Phonon modes at point G	
Eu	4c	$2A_g+A_u+B_{1g}+2B_{1u}+2B_{2g}+B_{2u}+B_{3g}+2B_{3u}$	
Er	4c	$2A_g+A_u+B_{1g}+2B_{1u}+2B_{2g}+B_{2u}+B_{3g}+2B_{3u}$	
Cu	4c	$2A_g+A_u+B_{1g}+2B_{1u}+2B_{2g}+B_{2u}+B_{3g}+2B_{3u}$	
S	4c	$2A_g+A_u+B_{1g}+2B_{1u}+2B_{2g}+B_{2u}+B_{3g}+2B_{3u}$	
S	4c	$2A_g+A_u+B_{1g}+2B_{1u}+2B_{2g}+B_{2u}+B_{3g}+2B_{3u}$	
S	4c	$2A_g+A_u+B_{1g}+2B_{1u}+2B_{2g}+B_{2u}+B_{3g}+2B_{3u}$	
Classification of modes			
$G_{ram}=12A_g + 6B_{1g} + 12B_{2g} + 6B_{3g}$	$G_{ir}=11B_{1u} + 5B_{2u} + 11B_{3u}$ (acoustic modesare not included)	$G_{ac}=B_{1u}+B_{2u}+B_{3u}$	$G_{meh}= 12A_g + 6A_u + 6B_{1g} + 12B_{1u} + 12B_{2g} + 6B_{2u} + 6B_{3g}+12B_{3u}$
Raman tensors			
$A_g\begin{bmatrix}0 & d & 0\\ d & 0 & 0\\ 0 & 0 & 0\end{bmatrix}$	$B_{1g}\begin{bmatrix}0 & 0 & e\\ 0 & 0 & 0\\ e & 0 & 0\end{bmatrix}$	$B_{2g}\begin{bmatrix}0 & 0 & 0\\ 0 & 0 & f\\ 0 & f & 0\end{bmatrix}$	$B_{3g}\begin{bmatrix}a & 0 & 0\\ 0 & b & 0\\ 0 & 0 & c\end{bmatrix}$

Lattice dynamics calculations were performed for providing the full-value interpretation of the observed vibrational spectra.

Returning back to Fig. 6, we note that luminescence contribution observed in the range above 300 cm^{-1} is easily assignable to the transition from excited electronic energy level $^2H_{11/2}$ of Er^{3+} ion to the ground state. Luminescence from $^4S_{3/2}$ and $^4F_{9/2}$ levels of Er^{3+} ion is also detected, while no detectable luminescence from excited states of Eu^{3+} ion were observed. This is the spectroscopic evidence of the purity of valence states Er^{3+} and Eu^{2+} earlier derived from the XRD data.

3.5 Ab initio Lattice Dynamics Calculations and the Interpretation of Observed Vibrational Spectra

The types of phonon modes were determined and the involvement of ions in vibrational modes was evaluated based on the displacement vectors derived from ab initio calculations (Tables 8-10). In the IR spectrum (Table8), rare-earth ions are appreciably involved in low-frequency modes.

The europiumis involved in the modes with frequencies up to 133 cm^{-1}. The B_{2u} mode at 93 cm^{-1} involves both Eu and Er. The erbium is involved in the modes with frequencies of up to 145 cm^{-1}. Copper vibrations appear in the IR modes with frequencies of up to 294 cm^{-1}. The greatest involvement of copper is in the 117.6 cm^{-1}(B_{1u}), 118.1 cm^{-1}(B_{2u}), and 129 cm^{-1} (B_{3u}) modes. The sulfur is involved in all IR modes. The 320.5 cm^{-1}(B_{1u}) and 324 cm^{-1} (B_{3u}) high-frequency IR modes mostly arise from sulfur vibrations. Three more modes can be distinguished at 243, 245, and 258 cm^{-1} (B_{2u}, $B_{1u,}$ and $B_{3u,}$ respectively), also arising from sulfur vibrations. Thus, the IR modes that arise from sulfur vibrations solely can be distinguished. For other ions, such modes are difficult to distinguish; every mode involves several ions of different types. For example, the low-frequency IR mode (B_{3u}, 62 cm^{-1}) involves all ions (Eu, Er, Cu, and S), and it is difficult to distinguish the dominant contribution from any one of them. However, this mode has a low intensity. According to the calculations, the 212.9 cm^{-1} (B_{2u}), 213.4 cm^{-1} (B_{3u}), and 259 cm^{-1} (B_{1u}) modes have high intensities. The sulfur is substantially involved in these modes.

Table 8.

Calculated IR vibrational frequencies (v_{calc}, cm^{-1}) and intensities (I_{calc}, km/mol) in $EuErCuS_3$.

Vibrations	v_{calc}	I_{calc}	Involved ions	Vibrations	v_{calc}	I_{calc}	Involved ions
B_{3u}	62	36,09	Eu, Er, Cu, S1, S2, S3	B_{2u}	243	640,72	S1, $S2^S$
B_{1u}	65	1,82	Eu^S, S1, S2	B_{1u}	245	69,05	$S1^S$, S2,S3
B_{2u}	93	11,69	Eu^S, Er^S, Cu, $S2^W$, S3	B_{3u}	258	506,11	S1, S2, $S3^S$
B_{3u}	100	28,43	Eu, Er, Cu, S1, S2,S3	B_{1u}	259	1447,84	Er^W,Cu^W,S1,S2,S3
B_{3u}	105	62,48	Eu^S, Er, Cu, S1, S2, S3	B_{3u}	269	37,9	Cu,S1, S2,$S3^S$
B_{1u}	112	25,84	Er, Cu, S1, S2, $S3^W$	B_{1u}	279	106,85	Cu, S1, S2,$S3^S$
B_{1u}	117,6	0,18	Eu, Er, Cu^S, S1, S2	B_{3u}	290	0,62	Cu, S1, $S2^S$,S3
B_{2u}	118,1	47,99	Eu, Cu^S, S3	B_{2u}	294	251,33	Cu,$S3^S$

B_{3u}	123,6	10,73	Eu, Cu, S1, S2	B_{1u}	300	10,08	S1, $S2^S$,$S3^S$
B_{3u}	129	148,97	Er, Cu^S, S1, S2,S3	B_{1u}	309	20,55	Cu^W, $S1^S$, S2, S3
B_{1u}	133	430,77	Eu^S, Er, Cu, S1, S2	B_{3u}	311	14,18	Cu^W, S1, $S2^S$, S3
B_{1u}	145	1,66	Er^S, S1, S2,S3	B_{1u}	320,5	12,41	S1, S2,$S3^S$
B_{2u}	212,9	1950,47	Er^W, S1, S2	B_{3u}	324	0,16	$S1^S$, S2,$S3^S$
B_{3u}	213,4	2113,62	Er^W, Cu^W, S1, S2,S3				

Notations: «s» stands for a strong and «w» for a weak displacement of ions involved in the mode

According to the calculations, the lowest-frequency Raman mode (A_g, 31 cm^{-1}) considerably involves erbium and europium (Table9). A considerable involvement of erbium is in the first four low-frequencymodes at31 cm^{-1} (A_g), 47 cm^{-1} (A_g), 56 cm^{-1} (B_{1g}), and 67.8 cm^{-1} (B_{3g}) and in two higher frequency B_{2g} modes at 95 and 160 cm^{-1}. In the Raman modes with frequencies higher than 160 cm^{-1}, erbium is involved only insignificantly. Europium is strongly involved in the modes with frequencies of up to 86 cm^{-1}; its involvement in higher-frequency modes is far weakerand is only insignificant after 160 cm^{-1}. Thus, both erbium and europium appear in the modes with frequencies of up to 160 cm^{-1}. Erbium is the major participant in the B_{1g} mode at 56 cm^{-1} (however, this mode has a very low intensity according to the calculations), while in the B_{2g} mode at 86 cm^{-1}, europium is. A considerable involvement of copper is in the modes with frequencies of up to 128 cm^{-1}. In the modes with frequencies higher than 218 cm^{-1}, copper involvement is weak. Sulfur is involved in all Raman modes. However, modes dominated by sulfur ions appear at 216,5 cm^{-1} (B_{3g}), 216.6 cm^{-1} (B_{1g}), 246 cm^{-1} (B_{1g}), 249 cm^{-1} (B_{3g}), 257 cm^{-1} (A_g), 277 cm^{-1} (A_g), 303 cm^{-1} (B_{2g}), 320.7 cm^{-1} (B_{2g}), and 325 cm^{-1} (A_g). The strongest Raman mode according to the calculations is the 325-cm^{-1} (A_g) mode, arising from sulfur ions. The 317 cm^{-1} (A_g) and 302 cm^{-1} (B_{2g}) modes, in which sulfur is strongly involved and copper is involved, too, but only weakly, also have high intensities.

The A_u modes, which are IR- and Raman-inactive, were also obtained by the calculations (Table 10). In the low-frequency A_u mode (68.5 cm^{-1}), erbium involvement is considerable; erbium is also involved in the third lowest frequency mode (111 cm^{-1}). In the 80.5-cm^{-1} mode, europium appears. The A_u modes with frequencies higher than 111 cm^{-1} almost do not involve rare-earth ions, but the involvement of sulfur in them is considerable.

Table 9.

Calculated Raman vibrational frequencies (v_{calc}, cm^{-1}) in $EuErCuS_3$.

Vibrations	v_{calc}	Involved ions	Vibrations	v_{calc}	Involved ions
		Eu^S, Er^S, Cu, S1,			$S1^S$, S2
A_g	31	$S2^S$,S3	B_{3g}	216,5	
		Eu, Er^S, Cu^S, S1,			$S1^S$, S2,S3
A_g	47	S2,$S3^S$	B_{1g}	216,6	
		Er^S, Cu, S1, S2,S3			Er^W, Cu, $S1^S$,
B_{1g}	56		A_g	218	$S2^S$,S3
		Eu, Er^S, Cu, S1,			S1, $S2^S$
B_{3g}	67,8	S2,S3	B_{1g}	246	
		Eu^S, Er^W, Cu^S, S1,			Cu^W, $S1^S$, S2,S3
A_g	76	S2,S3	B_{2g}	247	
		Eu^S, Er, Cu, S1,			S1, $S2^S$
B_{3g}	77	$S2^W$,S3	B_{3g}	249	
		Eu^S, Er, Cu^W, S1,			Cu^W, S1, $S2^S$,S3
B_{2g}	79	S2,S3	B_{2g}	255	
B_{1g}	80,3	Eu^S,Cu, S1, $S2^W$, S3	A_g	257	S1, S2,$S3^S$
B_{2g}	86	Eu^S, S2	A_g	270	Cu, S1, $S2^W$,$S3^S$
B_{2g}	95	Er^S, Cu, S1, S2,S3	A_g	277	$S1^S$, $S2^S$
B_{1g}	115,8	Eu^w, Er^w, Cu^S,S3	B_{3g}	291	Cu^W,$S3^S$
B_{2g}	116,3	Er^w, Cu^S,S2	B_{1g}	296	Cu^W,$S3^S$
B_{3g}	117,9	Eu, Cu^S,S3	B_{2g}	302	Cu^W, S1, $S2^S$,$S3^S$
A_g	122	Eu, Er, Cu, S1, S2	B_{2g}	303	$S1^S$, S2,$S3^S$
B_{2g}	123,9	Cu^S, $S1^S$, S3	A_g	317	Cu^W, S1, $S2^S$,S3
A_g	128	Eu, Er^W, Cu^S, S2,S3	B_{2g}	320,7	$S1^S$, S2,$S3^S$
A_g	137	Eu, Er, Cu, S1, S2	A_g	325	$S1^S$, S2,S3
B_{2g}	160	Eu, Er^S, $S1^W$, $S2^W$	B_{2g}	328	Cu^W, S1, $S2^S$,S3

Table 10.

Vibrational frequencies (v_{calc}, cm^{-1}) of Raman silent modesin $EuErCuS_3$

Vibrations	v_{calc}	Involved ions
A_u	68,5	Er^S, Cu^W, S1, S2, $S3^W$
A_u	80,5	Eu^S, Er^W, Cu, $S2^W$, S3
A_u	111	Eu, Er^S, S3

A_u	211	$S1^S$, S2, S3
A_u	244	$S1^S$, S2
A_u	292	Cu^W, $S3^S$

A comparison of the vibrational frequencies of Raman- and IR-active modes calculated in terms of DFT with the B3LYP functional with the experimental data appear in Figs.6 and 7.

The calculated IR absorption spectrum agrees with the observed one. The low-frequency IR modes involve all ions (Eu, Er, Cu, and S), and it is difficult to distinguish the dominant contribution from any one of them.The strongest lines, according to the calculations, are associated with sulfur vibrations and appear in the range from 210 to 260 cm^{-1}. The low-frequency Raman vibrations are also associated with the vibrations of all ions (lattice vibrations). So, the observed 102-cm^{-1} mode is assigned to lattice vibrations. The vibrations in the range 270-300 cm^{-1} have not been identified. According to the calculations, the high-frequency modes are associated with strong displacements of sulfur ions, so the high-frequency vibrations that appear in the observed spectrum in the range 450-490 cm^{-1} are assigned to the vibrations of sulfur ions.

3.6. Electronic Structure Calculations and Bandgap Measurement

The band structure obtained in terms of DFT with the B3LYP functional appears in Fig. 8. The bandgap was calculated to be 2.56 eV. According to the calculations (HOMO-LUMO), the band gap is direct (Γ-Γ). For europium and erbium, pseudo-potentials were used in the calculations to replace their core shells, including 4f. $EuErCuS_3$ is a mid-gap, direct-bandgap semiconductor.

Fig. 9 presents Kubelka-Munk function extracted from the measured diffuse reflection spectrum of $EuErCuS_3$.

The agreement between the experimental value of E_g and the calculated one is not perfect, however, it can be considered as a satisfactory

one. Additionally, the position of $H_{13/2}$ energy level of Er^{3+} ion within the bandgap can be extracted from reflectance spectra. This energy level is observable as the narrow peak at the left side of Kubelka-Munk function, and the maximum of this peak lies at 1.546 micron (6468 cm^{-1}), approximately in the same region where Er luminescence of Er ion is observed in oxides [51].

4. Conclusions

This article addresses the synthesis, structure, optical, magnetic, durometric, and thermal properties of the new complex sulfide $EuErCuS_3$. The compound crystallizes in a Eu_2CuS_3-type structure, which is typical of the $EuLnCuS_3$ compounds that contain mid-series lanthanides from samarium to erbium. $EuErCuS_3$, which contains the magnetic ion Er^{3+}, experiences a ferrimagnetic transition at 4.8 K. The compound experiences three reversible polymorphic transitions in the temperature range 1524-1720 K. It melts in congruently at 1740 K. The magnetic and thermal properties of $EuErCuS_3$ agree with the data published for the $ALnCuS_3$ (A = Sr, Eu; Ln = La-Lu) isostructural compounds [7,12,13]. Ab initio crystal structure and phonon spectrum calculations have been performed for $EuErCuS_3$ in terms of the LCAO-MO approach, density functional theory with the B3LYP hybrid functional.The results of the calculations enabled us to interpret the observed vibrational spectra.

Supporting Information

Structural cif file; atom coordinates; bond lengths; raman, luminescence and IR spectra; SEM micrograph; thermal curves.

Author contributions

All authors reviewed and commented on the manuscript.

Acknowledgements

The work was supported by the State budget allocated to the fundamental research in the Ministry of Science and Education, Russian Federation of (Project No. V.45.3.3), and supported by RFBR Grant 17-02-00754, and supported by the Ministry of Science and Higher Education of the Russian Federation under Project No 3.9534.2017/8.9.

References

[1] L.A. Koscielski, J.A. Ibers, The structural chemistry of quaternarychalcogenides of the type AMM‘Q_3, Z. Anorgan. Allgem. Chem. 638 (2012) 2585–2593.doi: 10.1002/zaac.201200301

[2] T.D. Brennan, J.A. Ibers, $LaPbCuS_3$: Cu(I) insertion into the *a*-La_2S_3 framework, J. Solid State Chem. 97 (1992) 377–382. doi:10.1016/0022-4596(92)90046-X

[3] L.D. Gylay, I.D. Olekseyuk, M. Wolcyrz, J. Stepien-Damm, Crystal structures of the $RCuPbS_3$ (R = Tb, Dy, Ho, Er, Tm, Yb and Lu) compounds, J. Alloys Comp. 399 (2005) 189-195. doi:10.1016/j.jallcom.2005.03.036

[4] S.T. Bairamova, M.R. Bagieva, S.M. Agapashaeva, O.M. Aliev, Synthesis and Properties of Structural Analogs of the Mineral Bournonite, Inorganic Materials. 47 (2011) 345–348.doi:10.1134/S0020168511040054

[5] M. Ohta, S. Hirai, T. Mori, Y. Yajima, T. Nishimura, K. Shimakage, Effect of nonstoichiometryon thermoelectric properties of γ-Tb_2S_{3-x}, J. Alloys Compd. 418(2006) 209–212. doi:10.1016/j.jallcom.2005.10.065

[6] M. Ohta, H. Yuan, S. Hirai, Y. Yajima, T. Nishimura, K. Shimakage, Thermoelectric properties of Th_3P_4-type rare-earth sulfides Ln_2S_3 (Ln = Gd, Tb) prepared by reaction of their oxides with CS_2 gas, J. Alloys Compd. 451 (2008)627–631.doi:10.1016/j.jallcom.2007.04.078

[7] A.V. Ruseikina, O.V. Andreev, E.O. Galenko, S.I. Koltsov, Trends in thermodynamic parameters of phase transitions of lanthanide sulfides $SrLnCuS_3$ (Ln = La–Lu), J. Therm. Anal. Calorim. 128 (2017) 993–999.doi: 10.1007/s10973-016-6010-9

[8] Yu.A. Murashko, A.V. Ruseikina, A.A. Kislitsyn, O.V. Andreev, Optical and Thermal Properties of the $EuLnCuS_3$ (Ln = La, Pr, Sm, Gd), Inorg. Materials. 51 (2015) 1213-1218. doi:10.1134/S0020168515120079

[9] R.M. Rojas, M.J. Torralvo, L.C. Otero-Diaz, Thermal behaviour and microstructural characterization of lanthanide sulphides, J. Therm.Anal. Calorim. 38 (1992) 961–971.https://doi.org/10.1007/BF01979429

[10] K. Matsumoto, L. Li, , S. Hirai, E. Nakamura, D. Murayama, Y. Ura, , S. Abe, Large magnetocaloric effect in sintered ferromagnetic EuS, Cryogenics (2016), http://dx.doi.org/10.1016/j.cryogenics.2016.08.001

[11] A.V. Ruseikina, L.A. Solov'ev, O.V.Andreev, Crystal structures and properties of $SrLnCuS_3$ (Ln = La, Pr), Russ. J. Inorg. Chem.59 (2014) 196–201. doi: 10.1134/S0036023614030188.

[12] M. Wakeshima, F. Furuuchi, Y. Hinatsu, Crystal structures and magnetic properties of novel rare-earth copper sulfides, $EuRCuS_3$ (R = Y, Gd–Lu), J. Phys: Condens Matter. 16 (2004) 5503–5518.doi:10.1088/0953-8984/16/30/012

[13] F. Furuuchi, M. Wakeshima, Y. Hinatsu, Magnetic properties and (151) Eu Mossbauer effects of mixed valence europium copper sulfide Eu_2CuS_3, J. Solid State Chem. 177 (2004) 3853–3858. doi:10.1016/j.jssc.2004.04.034

[14] P. Wu, A.E. Christuk, J.A. Ibers, New Quaternary Chalcogenides $BaLnMQ_3$ (Ln = Rare Earth; M = Cu, Ag; Q=S, Se). Structure and Property Variation vs Rare-Earth Element, J. Solid State Chem. 110 (1994) 337-344.doi: 10.1006/jssc.1994.1177

[15] A.V. Ruseikina, O.V. Andreev, Regularities of Change in the Structural Parameters of $EuLnCuS_3$ (Ln = La–Nd, Sm, Gd, Ho),Russ. J. Inorg. Chem. 62 (2017) 160–167.doi:10.1134/S0036023617020140

[16] A.V. Ruseikina, O.V. Andreev, Phase Equilibria in the Cu_2S–La_2S_3–EuS System, Russ. J. Inorg. Chem. 62 (2017) 610–618. doi: 10.1134/S0036023617050199

[17] A.V. Ruseikina, Zh. A. Demchuk, Crystal structure and properties of $AHoCuS_3$ (A = Sr or Eu), Russ. J. Inorg. Chem. 62 (2017) 27-32. doi:10.1134/S0036023617010168

[18] A.V. Ruseikina, O.V. Andreev, Phase Equilibria in Systems $DyCuS_2$–EuS and Cu_2S−Dy_2S_3−EuS, Russ. J. Inorg. Chem. 63 (2018) 1494–1500.doi: 10.1134/S0036023618110141

[19] W. Cook, L. Shiozawa, F. Augustine, The Cu-S Phase Diagram, J. Appl. Phys. 41 (1970) 3058-3063.

[20] D.J. Chakrabarti, D. E. Laughlin, The Cu-S (Copper-Sulfur) System, Bulletin of Alloy Phase Diagrams 4 (1983) 254-271. https://link.springer.com/content/pdf/10.1007/bf02868665.pdf

[21] L. Li, S. Hirai,E. Nakamura, H. Yuan, Influences of Eu_2O_3 characters and sulfurization conditions on the preparation of EuS and its large magnetocaloric effect, J. Alloys Compd.687 (2016) 413-420.http://dx.doi.org/10.1016/j.jallcom.2016.06.053

[22] L. Li, S. Hirai, H. Yuan, Influences of Yb_2O_3 characters and sulfurization conditions on preparation of Yb_2S_3, J. Alloys Compd.618 (2015) 742–749. http://dx.doi.org/10.1016/j.jallcom.2014.08.109

[23] T. Schleid, F. Lissner, Einkristalle von A-Nd_2S_3, U-Ho_2S_3, D-Er_2S_3 und E-Lu_2S_3 durch Oxidation reduzierter Chloride der Lanthanide mit Schwefel, Z. Anorgan. Allgem. Chem. 615 (1992) 19 26.https://doi.org/10.1002/zaac.19926150905

[24] C.M. Forster, W.B. White, Optical absorption edge in rare earth sesqui sulfides, Mater. Res. Bull. 41 (2006) 448-454. https://doi.org/10.1016/j.materresbull.2005.07.035

[25] V.A. Obolonchik, L.A. Ivanchenko,Properties of europium chalcogenides. Scientificthought, Kiev, 1980.

[26] K.G. Subhadra, Rao B. Raghavendra, D.B. Sirdeshmukh, X-ray determination of the Debye-Waller factors and Debye temperatures of europium monochalcogenides. Pramana- J. Phys. 38 (1992) 681–683. doi:10.1007/bf02875064

[27] P. P. Fedorov, Anneal time determined by studying phase transitions in solid binary systems,Russ. J. Inorg. Chem.37 (1992) 973-968

[28] J.W. Visser, A fully automatic program for finding the unit cell from powder data, J. Appl. Cryst. 2 (1969) 89-95. https://doi.org/10.1107/S0021889869006649

[29] P. Lemoine, D. Carré, M. Guittard, Structure du sulfured' europiumet de cuivre Eu_2CuS_3, ActaCrystallog. 42 (1986) 390-391.doi: 10.1107/S0108270186096063

[30] L.A. Solovyov, Full-profile refinement by derivative difference minimization, J. of Applied Crystallography. 37 (2004) 743-749.doi: 10.1107/S0021889804015638

[31] Brandenburg K. Diamond – Visual Crystal Structure Information System Crustal Impact, Postfach 1251, D-53002 Boon.

[32] A.G. Kolmakov, V.F. Terentyev, M.B. Bakirov, Hardness Measurement Methods, Second Edition, Intermet Engineering, Moscow, 2005. http://www.pseudology.org/science/Metody_izmer_tverdosti2.pdf

[33] D.A. Velikanov, Vibration magnetometer. RF patent for the invention № 2341810. Publ. 12.20.2008, Bulletin № 35 http://www.freepatent.ru/patents/2341810

[34] D.A.Velikanov, Magnetometer with a superconducting quantum interferometric sensor. RF patent for the invention № 2481591. Publ. 10.05.2013, Bulletin № 13. http://www.freepatent.ru/patents/2481591

[35] V. G. Tsirelson, Quantum chemistry. Molecules, molecular systems and solids, third edition, Binom. KnowledgeLab, Moscow, 2014.

[36] A.D. Becke, Density-functional thermochemistry. III. The role of exact exchange, J. Chem. Phys. 98 (1993) 5648-5652.doi: 10.1063/1.464913

[37] P.L. Stephens, F.J. Devlin, C.F. Chabalowski, M.J. Frisch, Ab Initio Calculation of Vibrational Absorption and Circular Dichroism Spectra Using Density Functional Force Fields, J. Phys. Chem. 98 (1994) 11623-11627. doi: 10.1021/j100096a001

[38] R. Dovesi, R. Orlando, A. Erba, C.M. Zicovich-Wilson, B. Civalleri, S. Casassa, L. Maschio, M. Ferrabone, M. De La Pierre, P. D'Arco, Y. Noel, M. Causa, M. Rerat, B. Kirtman,Crystal14: A Program for the Ab Initio Investigation of Crystalline Solids, Int. J. Quantum Chem. 114 (2014) 1287-1317.doi:10.1002/qua.24658

[39] Crystal. http://www.crystal.unito.it/index.php(accessed 29 October 2018).

[40] M. Dolg, H. Stoll, A. Savin, H. Preuss, Energy-adjusted pseudopotentials for the rare earth elements, Theor. Chim. Acta. 75 (1989) 173-194.doi: 10.1007/BF00528565

[41] M. Dolg, H. Stoll, H. Preuss, A combination of quasi relativistic pseudopotential and ligand field calculations for lanthanoid compounds, Theor. Chim. Acta 85 (1993)441-450.doi:10.1007/BF01112983

[42] Energy-consistent Pseudopotentials of the Stuttgart/Cologne Group. http://www.tc.uni-koeln.de/PP/clickpse.en.html (accessed 29 October 2018).

[43] K. Doll, N.M. Harrison, Chlorine adsorption on the Cu(111) surface, Chemical Physics Letters 317 (2000) 282-289.doi: 10.1016/S0009-2614(99)01362-7

[44] T. Ouazzani, A. Lichanot, C. Pisani and C. Roetti, Relaxation and electronic structure of surfaces in lithium sulphide: A Hartree-Fockab initio approach, J. Phys. Chem. Solids 54 (1993) 1603-1611.doi: 10.1016/0022-3697(93)90356-V

[45] V.A. Chernyshev, A.E. Nikiforov, V.P. Petrov, A.V. Serdtsev, M.A. Kaschenko, S.A. Klimin. Structure and Lattice Dynamics of Rare-Earth Ferroborate Crystals: Ab Initio Calculation, Phys. Sol. St. 58 (2016)1642-1650 doi: 10.1134/S1063783416080096

[46] V.A. Chernyshev, V.P. Petrov, A.E. Nikiforov, Lattice dynamics of rare-earth titanates with the structure of pyrochlore R2Ti2O7 (R = Gd, Tb, Dy, Ho, Er, Tm, Yb, and Lu): Ab initio calculation, Phys. Sol. St. 57 (2015) 996-1002 doi: 10.1134/S1063783415050078

[47] N.E. Brese and M. O'Keeffe. Bond-valence parameters for solids. Acta Cryst. B47 (1991) 192-197. doi.org/10.1107/S0108768190011041

[48] Néel L. Magnetism and Local Molecular Field, Science 174 (1971) 985-992.doi: 10.1126/science.174.4013.985

[49] N.V. Kudrevatykh, A.S. Volegov**,** Magnetism of rare earth metals and their intermetallic compounds, pub. UralUniversity, Yekaterinburg, 2015. http://elar.urfu.ru/bitstream/10995/36121/1/978-5-7996-1604-5_2015.pdf

[50] J. Jensen, A.R. Mackintosh. Rare Earth Magnetism. Structures and Excitations, Clarendon Press, Oxford, 1991.https://www.fys.ku.dk/~jjensen/Book/Ebook.pdf

[51] Xiao Xia Zhang, King Fai Li, Kok Wai Cheah, Xianju Zhou, Peter A. Tanner. 1.54 and 1.75 μm infrared luminescence of Y_2O_3:Er^{3+}. Chem. Phys. Lett. 400 (2004) 331–335.

Captions

Fig. 1. Measured (1), calculated (2), and difference (3) X-ray diffraction profiles of a $EuErCuS_3$ sample after DDM structure refinement. The bars indicate the peaks positions of the of major phase and Er_2O_2S.

Fig. 2. [010] perspective projections of the $EuErCuS_3$ structure.

Fig. 3. SEM micrograph and thermal curves for a $EuErCuS_3$ sample.

Fig. 4. Magnetic moment versus magnetic field for $EuErCuS_3$.

Fig. 5. Temperature-dependent reciprocal magnetic susceptibility for a $EuErCuS_3$ sample.

Fig. 6. Raman and luminescence spectra of a $EuErCuS_3$ crystal excited by 514.5- and 457.9-nm laser beams. The bars indicate the calculated Raman frequencies of $EuErCuS_3$.

Fig. 7. IR spectrum of $EuErCuS_3$. The bars indicate the calculated IR vibrational frequencies in $EuErCuS_3$. $EuErCuS_3$ is IR-transparent in the wavenumber window 4000–400 cm^{-1}.

Fig. 8. $EuErCuS_3$ band structure.

Fig. 9. Diffuse reflection spectra of $EuErCuS_3$.

Highlights

1. The $EuLnCuS_3$ compound exhibit ferrimagnetic properties at low temperature.
2. The polymorphic transitions for $EuLnCuS_3$ are identified at high temperature.
3. $EuErCuS_3$ is a wide-gap semiconductor.
4. Valence purity of Eu^{2+} is proved via both XRD and optical techniques
5. The ab initio calculation of the Raman and infrared spectra of $EuErCuS_3$, made for Pnma symmetry, agrees well with experiment.

Figure

Click here to download high resolution image

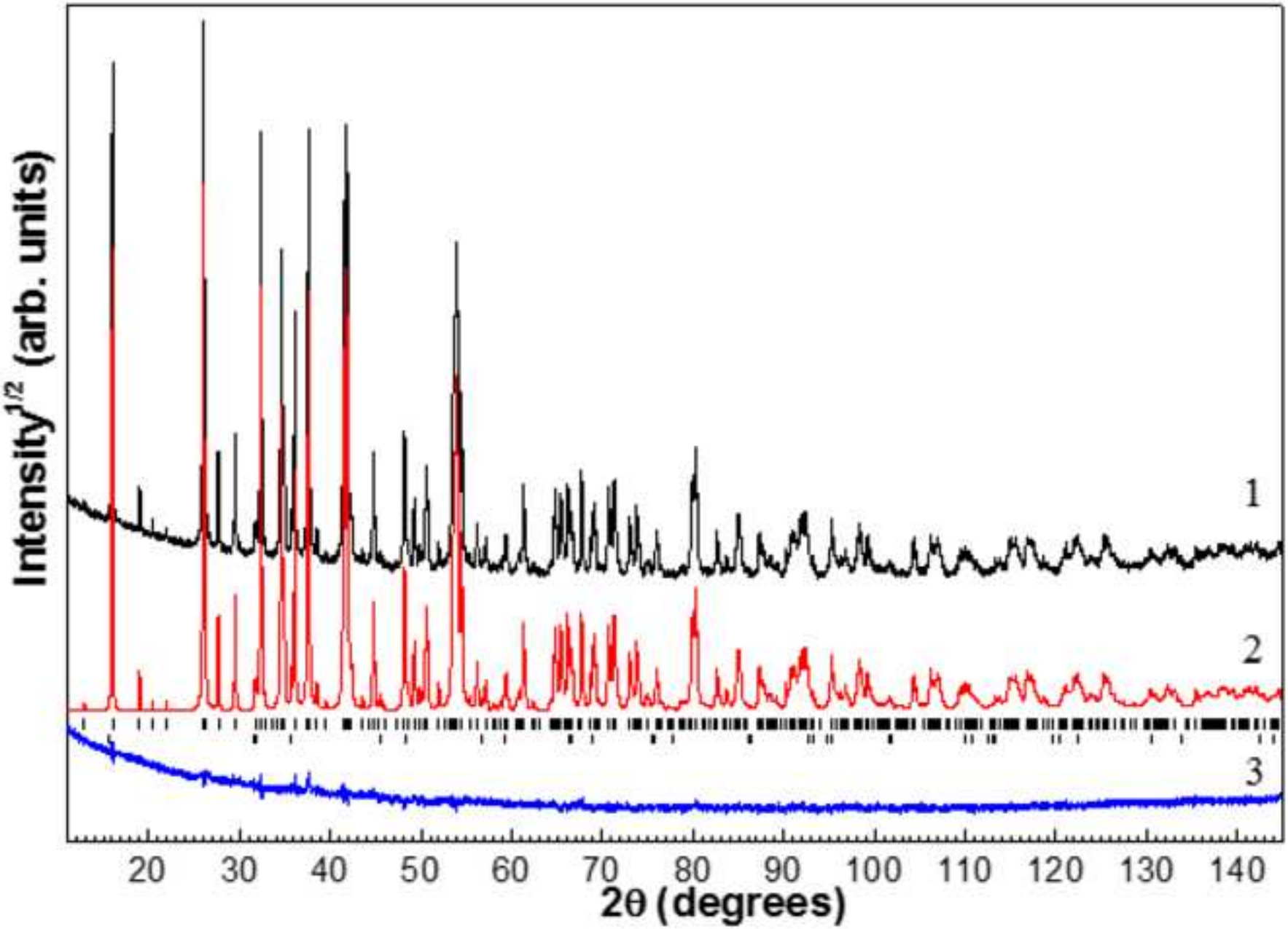

Figure

Click here to download high resolution image

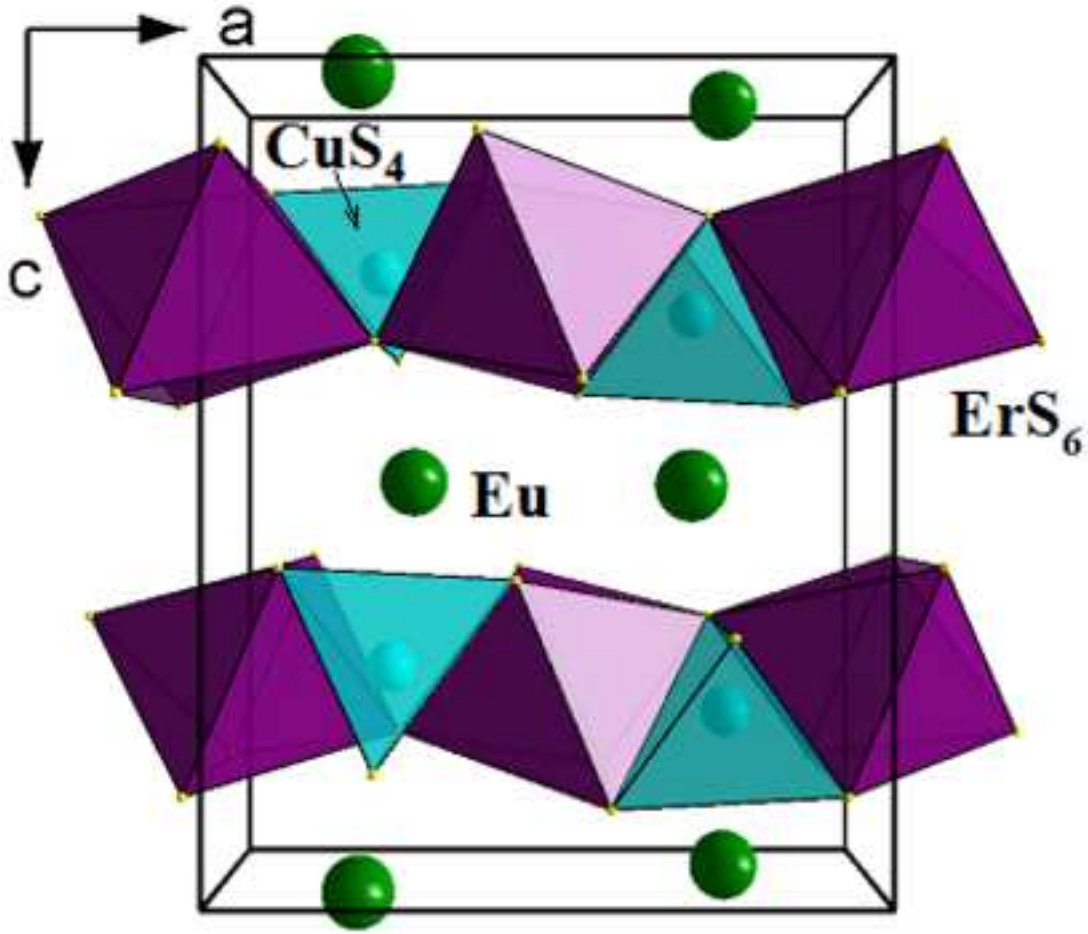

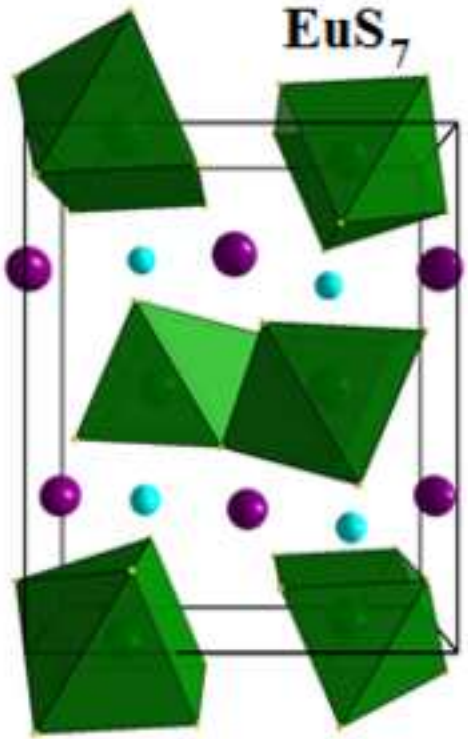

Figure
Click here to download high resolution image

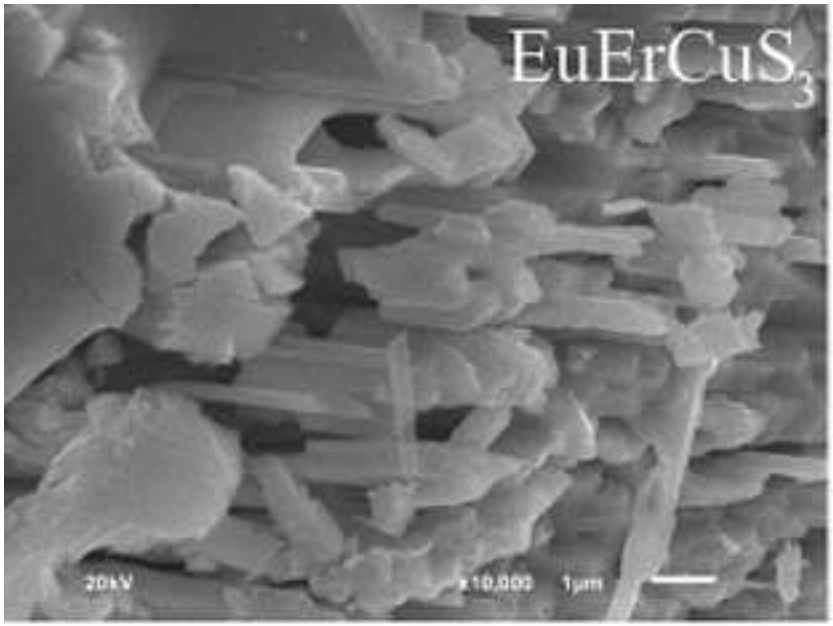

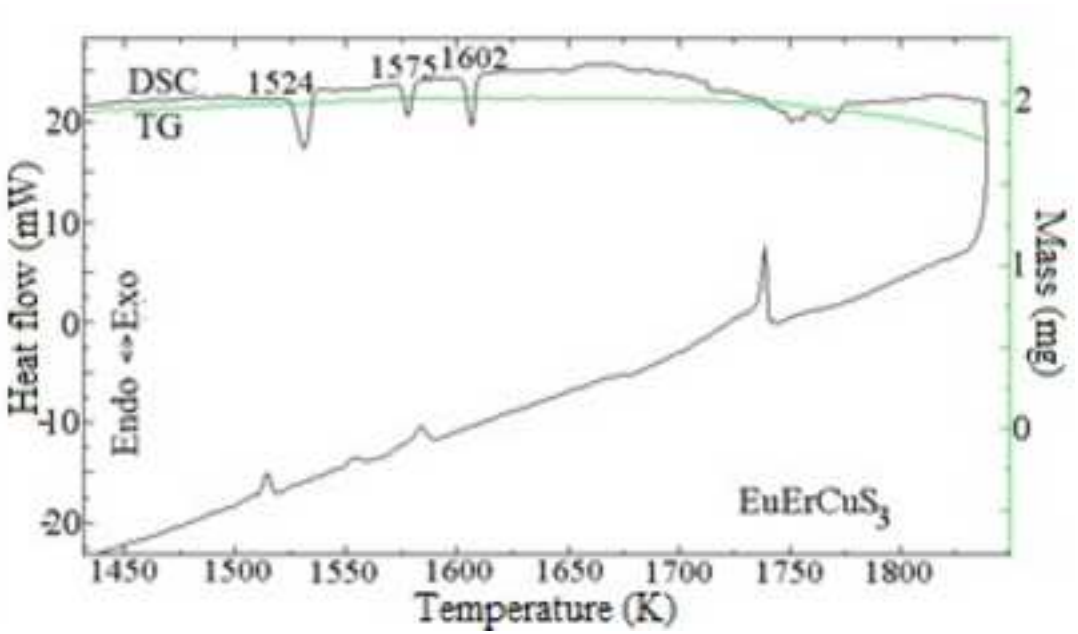

Figure

Click here to download high resolution image

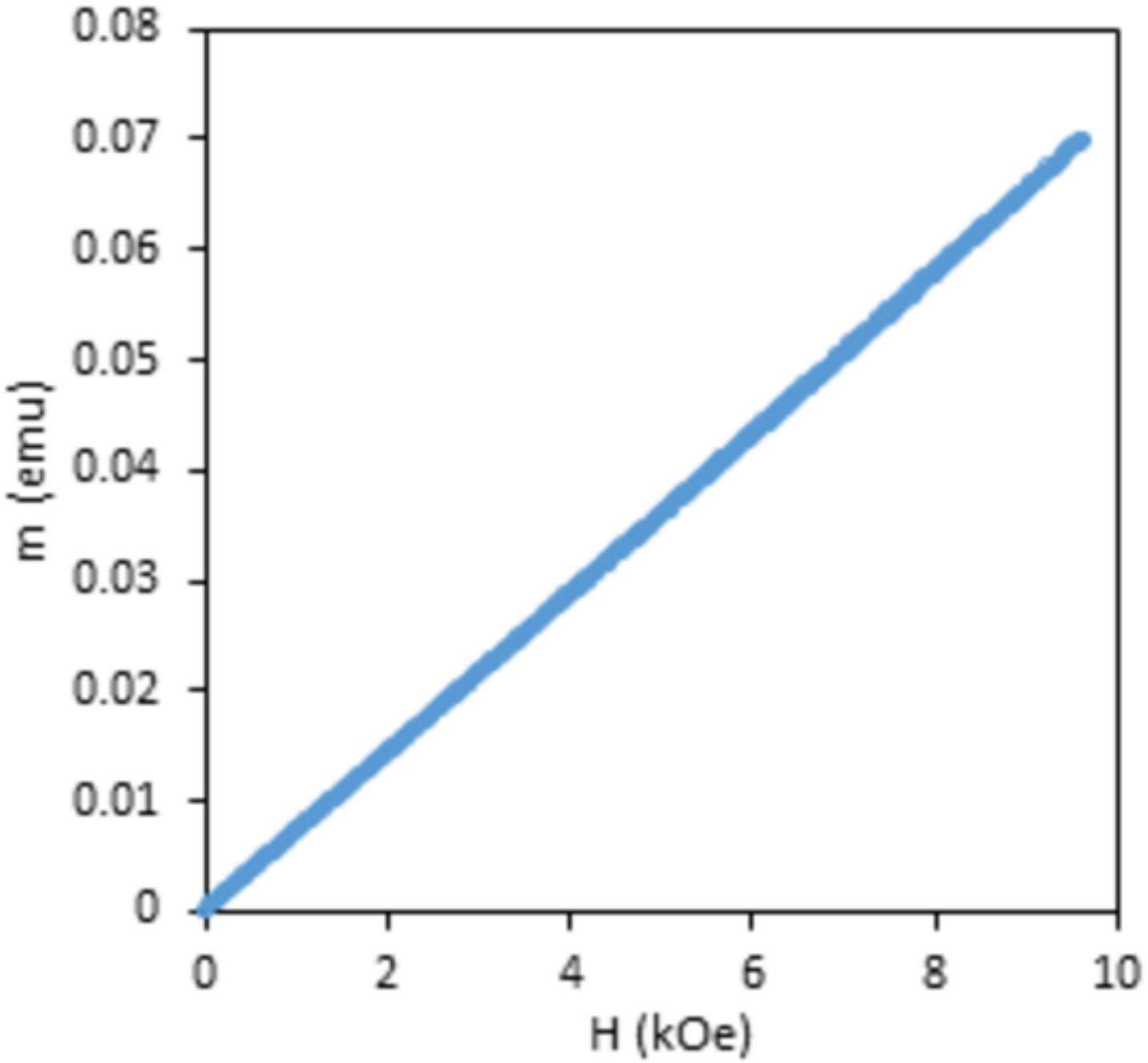

Figure

Click here to download high resolution image

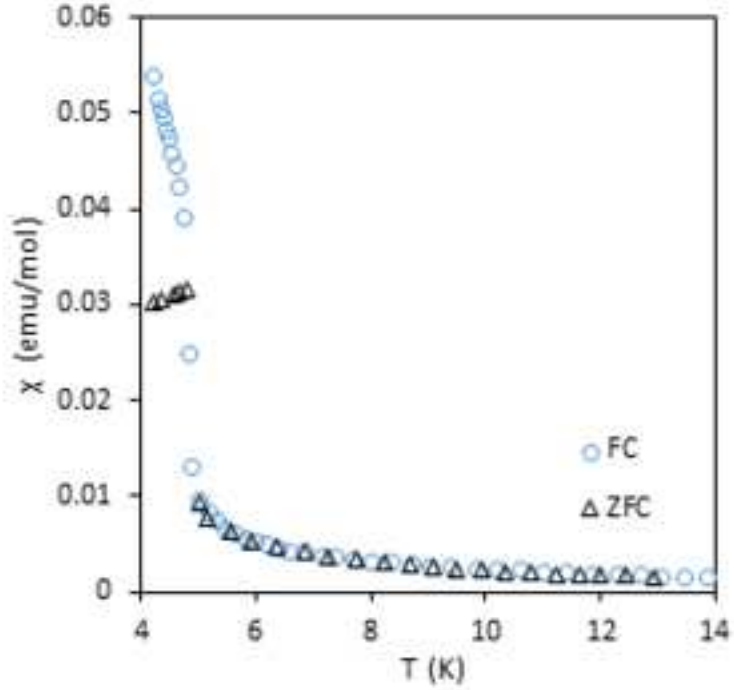

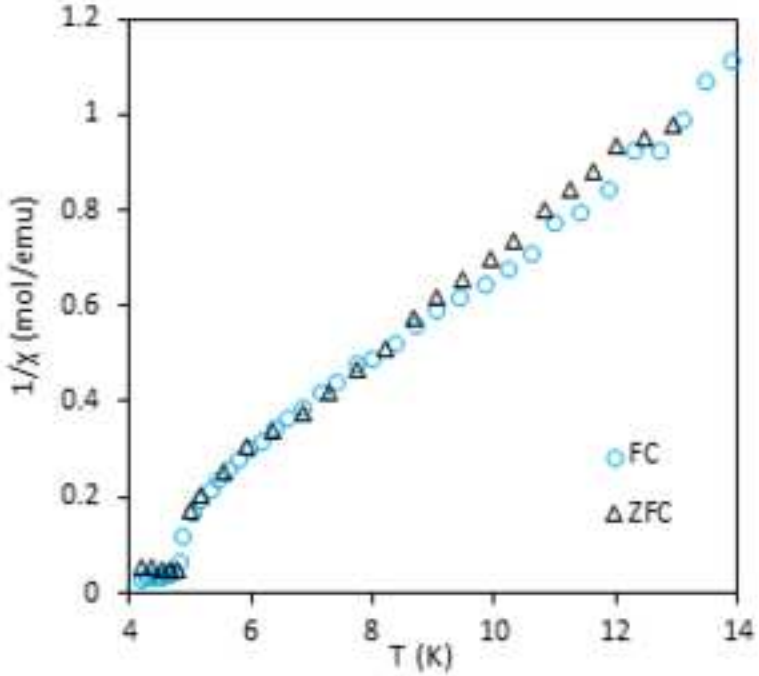

Figure
Click here to download high resolution image

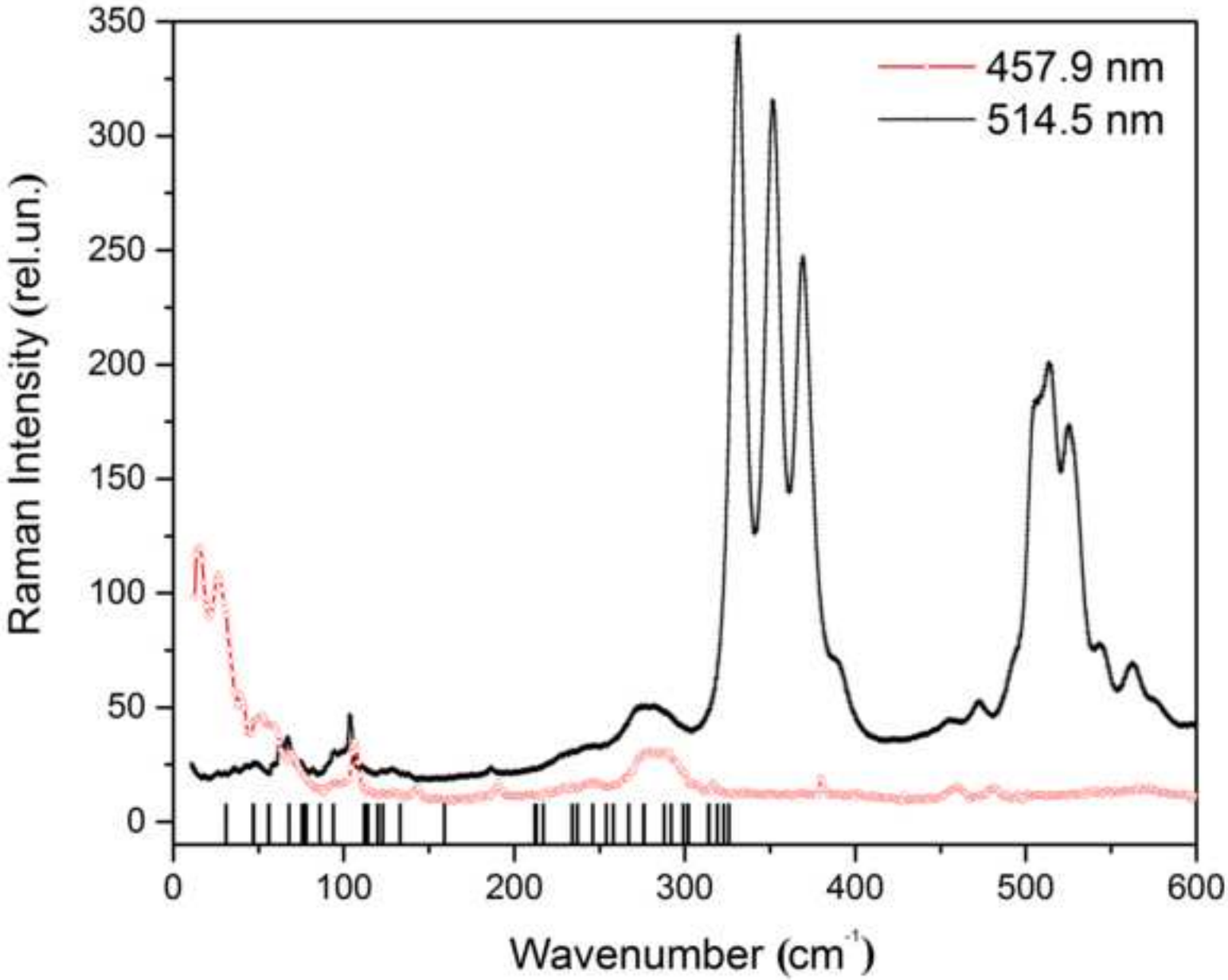

Figure

Click here to download high resolution image

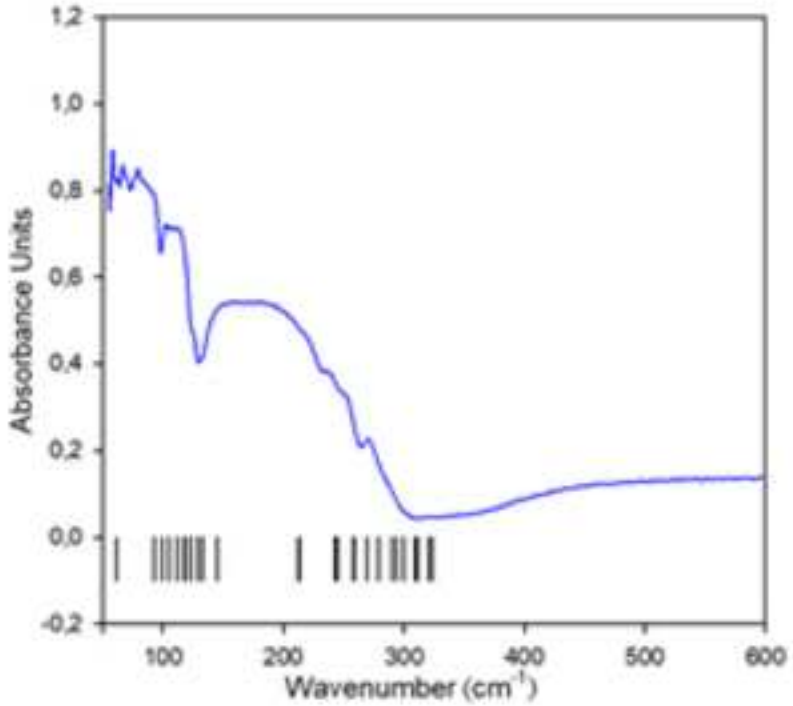

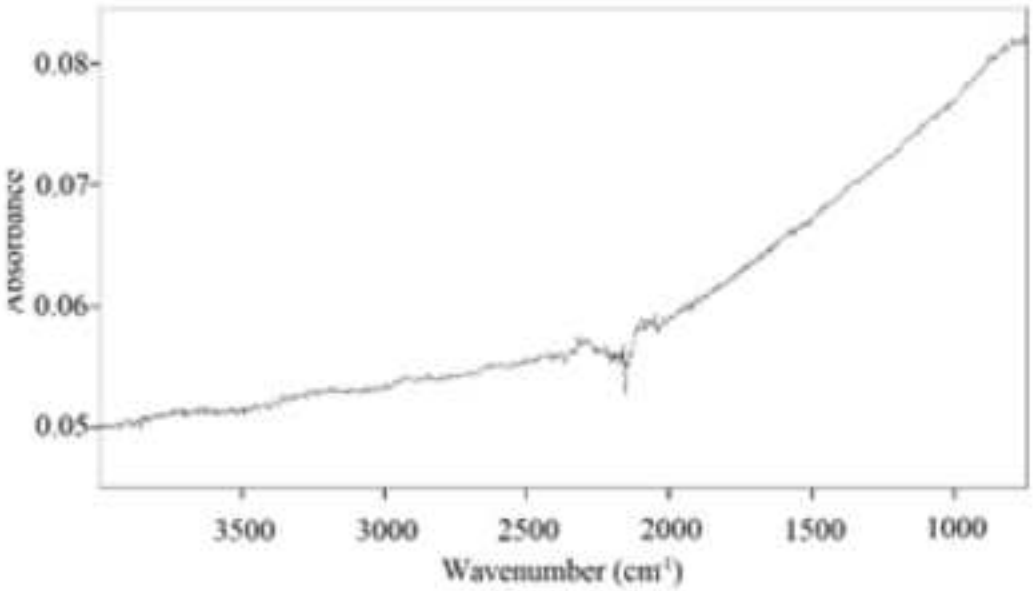

Figure
Click here to download high resolution image

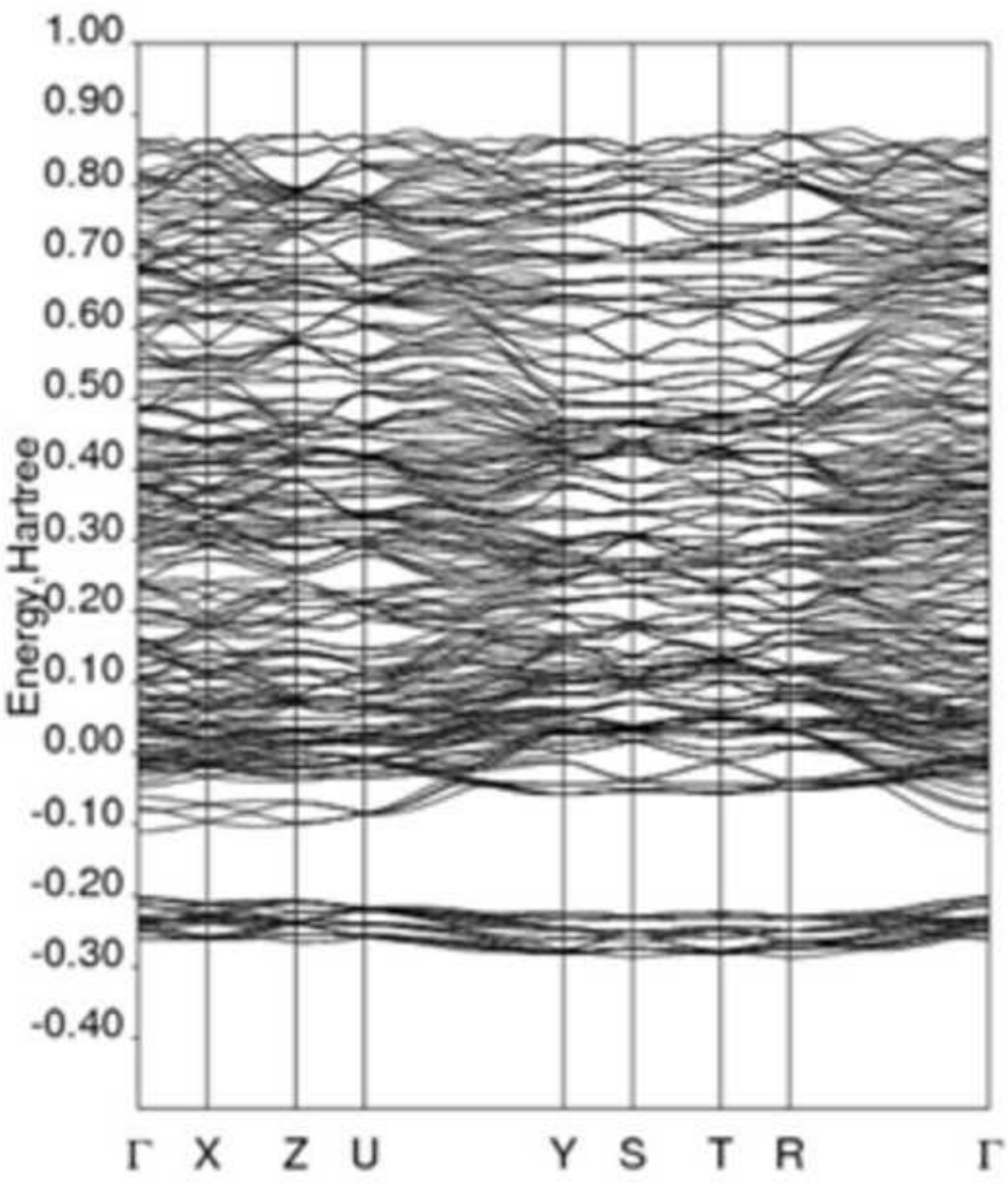

Figure

Click here to download high resolution image